Journal of Alloys and Compounds 604 (2014) 327–330

Contents lists available at ScienceDirect

Journal of Alloys and Compounds

journal homepage: www.elsevier.com/locate/jalcom

The oxygen octahedral distortion induced magnetic enhancement in multiferroic $Bi_{1-x}Yb_xFe_{0.95}Co_{0.05}O_3$ powders

Longsheng Chen, Yonghou He, Jiang Zhang, Zhongquan Mao, Yu-Jun Zhao, Xi Chen *

Department of Physics, South China University of Technology, Guangzhou 510640, China

ARTICLE INFO

Article history:
Received 16 January 2014
Received in revised form 21 March 2014
Accepted 21 March 2014
Available online 28 March 2014

Keywords:
$BiFeO_3$
Sol–gel method
Structural distortion
Dzyaloshinsky-Moriya interaction
Magnetism

ABSTRACT

The $Bi_{1-x}Yb_xFe_{0.95}Co_{0.05}O_3$ (x range from 0 to 0.25) powders have been prepared by the sol–gel method. A phase transition from rhombohedral *R*3*c* to orthorhombic *Pbnm* via a biphasic region has been observed. The Rietveld refinement and Raman scattering analyses suggest an increase of the rotation of the oxygen octahedra ω for $x \leqslant 0.05$. The remanent magnetization of $Bi_{1-x}Yb_xFe_{0.95}Co_{0.05}O_3$ is enhanced substantially at the *R*3*c* phase region. The enhancement of the magnetization is attributed to the augment of the Dzyaloshinsky-Moriya interaction and suppression of the spin cycloid, which is determined by ω.

1. Introduction

Magnetoelectric multiferroics are materials that show spontaneously not only magnetic and electric ordering but also the coupling between them [1,2]. They have renewed interest in the last decade due to the potential technological applications in data storage, spintronics, etc [3]. The only known room temperature magnetoelectric multiferroics, by far the most studied, is the rhombohedrally distorted perovskite $BiFeO_3$ (BFO) [4]. This material exhibits high ordering temperatures (the Néel temperature $T_N \sim 643$ K and the ferroelectric Curie temperature $T_C \sim 1103$ K) [3], excellent ferroelectric performance and conductive domain walls [5]. The outstanding properties make it a promising candidate for device integration.

The bulk BFO has spontaneous ferroelectric polarization along the diagonals of the perovskite unit cell [3], while it exhibits a G-type antiferromagnetic order with the magnetic moments of Fe^{3+} ions lying ferromagnetically within the pseudocubic (1 1 1) plane and antiferromagnetically between the adjacent planes [6]. Besides, the symmetry allows a weak canting of the antiferromagnetic sublattices due to the local magnetoelectric coupling to the polarization [3]. Such antiferromagnetic order is superimposed spontaneously with a long range spiral spin structure with a period of ~ 62 nm [7]. As a result the macroscopic magnetization and the linear magnetoelectric effect are inhibited [8], which becomes a big obstacle to the application of BFO. Theoretically, it has been shown that the Dzyaloshinsky-Moriya (DM) interaction causes the canting of the magnetic sublattices, and the DM vector is determined by the rotations of the oxygen octahedra [6]. Furthermore Zvezdin et al., investigated the effects of the displacement of the iron ions along the principal axis and transverse shift of the oxygen ions as well as the rotations of the oxygen octahedra, and suggested that these three basic distortions result in the coexistence of the spin canting and the cycloidal spin ordering [9].

Experimentally an effective way to enhance the magnetic properties of BFO is chemical doping [10–12]. Besides, the so called "chemical pressure" can be induced by substitution of Bi^{3+} ions with the rear earth (RE) ions, which leads to a significant structural distortion [3]. Yuan et al. reported subtle changes of the crystal axis and crystal axial angles in La doped BFO ceramics which lead to a structural transformation from rhombohedral *R*3*c* phase to pseudotetragonal *P*4/*mmm* phase [10]. Zhang et al. found a substitution-induced transition to an orthorhombic phase in Eu doped BFO, accompanied with a shrink of the lattice parameters and the volume of the unit cell [13]. It is believed that these structure distortions suppress the spin cycloid, which causes the enhancement of the magnetic properties of BFO [10,11,13]. However the structure distortions in these works were discussed rather roughly and the type of the distortion related to suppressing the spin cycloid was not clear. In this paper we demonstrate clearly that the enhanced magnetization of BFO is attributed to the augment of the DM interaction determined by the rotation of the oxygen octahedra.

* Corresponding author.
E-mail address: xichen@scut.edu.cn (X. Chen).

http://dx.doi.org/10.1016/j.jallcom.2014.03.108
0925-8388/

2. Experimental details

$BiFeO_3$ and $Bi_{1-x}Yb_xFe_{0.95}Co_{0.05}O_3$ (BYFCO) powders with doping concentration x range up to 0.25 are prepared by a sol–gel method, where Co is co-doped in order to improve the qualities of the BYFCO specimens. Stoichiometric amounts of $Bi(NO_3)_3{\cdot}5H_2O$, $Yb(NO_3)_3{\cdot}6H_2O$, $Fe(NO_3)_3{\cdot}9H_2O$ and $Co(NO_3)_2{\cdot}6H_2O$ are dissolved in dilute nitric acid respectively, and calculated amount of tartaric acid is added as a complexing agent. The resultant solution is evaporated and dried at 150 °C with continuous stirring and grinded in an agate mortar to obtain xerogel powders. Then the xerogel powders are preheated to 300 °C for an hour to remove excess hydrocarbons and NO_x impurities, and subsequently sintered at 600 °C for two hours. The crystal structure of the specimens are examined by a Bruker D8 ADVANCE X-ray diffractometer with Cu Kα radiation (λ = 1.5418 Å, Ni filter). The 2θ scans are taken at a rate of 2°/min (step size 0.02°) with 40 kV/40 mA power settings. The vibrational properties of the specimens are investigated using a Raman spectrometer (Renishaw 2000, resolution 1–2 cm^{-1}) in backscattering mode with a 633 nm He–Ne laser as the excitation source. Magnetic measurements are performed with a vibrating sample magnetometer (VSM) in a physical property measurement system (PPMS, Quantum Design). The specimens are pressed into pellets for M–H measurement with the magnetic field up to 80 kOe.

3. Results and discussion

Fig. 1 shows the X-ray diffraction (XRD) patterns of BFO and BYFCO powders. It is clear that BFO crystallized in a rhombohedral perovskite structure. A small trace amount of $Bi_2Fe_4O_9$ (JCPDS no. 72-1832) can be found in BFO. By codoping 5% amounts of Co and Yb into the specimens, the impurity phase $Bi_2Fe_4O_9$ is inhibited. All diffraction peaks in the low concentration doping region of $x < 0.08$ can be labeled based on a single *R*3*c* phase (JCPDS no. 82-1254). As shown in Fig. 1, new peaks (marked with upward arrows) emerge as $x \geqslant 0.08$ and grow up as x increases, which can be labeled based on an orthorhombic phase (JCPDS no. 74-1474). While the characteristic peaks (marked with downward arrows) of *R*3*c* phase become more and more weak and completely vanish in the region of $x \geqslant 0.2$. The XRD pattern of $Bi_{0.8}Yb_{0.2}Fe_{0.95}Co_{0.05}O_3$ is very similar to that of the orthorhombic $Bi_{1-x}Ho_xFeO_3$ [11]. Thereby, three different regions which can be sorted according to Fig. 1 indicate clearly the phase transitions in BYFCO.

Rietveld refinement analyses are performed on the XRD patterns using the GSAS program [14], in order to clarify the phase transitions in BYFCO. The results are illustrated in Fig. 2, with satisfactory refining quality $chi^2 \leqslant 2.348$, $R_{wp} \leqslant 5.57\%$ and $R_p \leqslant 4.33\%$. As shwon in Fig. 2(a), the structure of BYFCO changes from *R*3*c* phase at lower doping concentration ($x < 0.07$) to the biphasic (*R*3*c* + *Pbnm*) at intermediate concentration and finally to a pure *Pbnm* phase as $x > 0.18$. The lattice constants a_{pc} and c_{pc} [Fig. 2(b)] as well as the reduced unit cell volume V_{pc} [Fig. 2(c)]

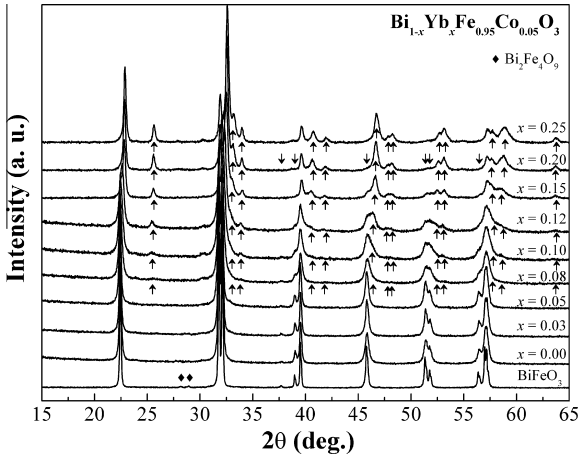

Fig. 1. XRD patterns of BFO and BYFCO powders. The upward arrows indicate the new peaks and the downward arrows indicate the vanishing peaks as x increases.

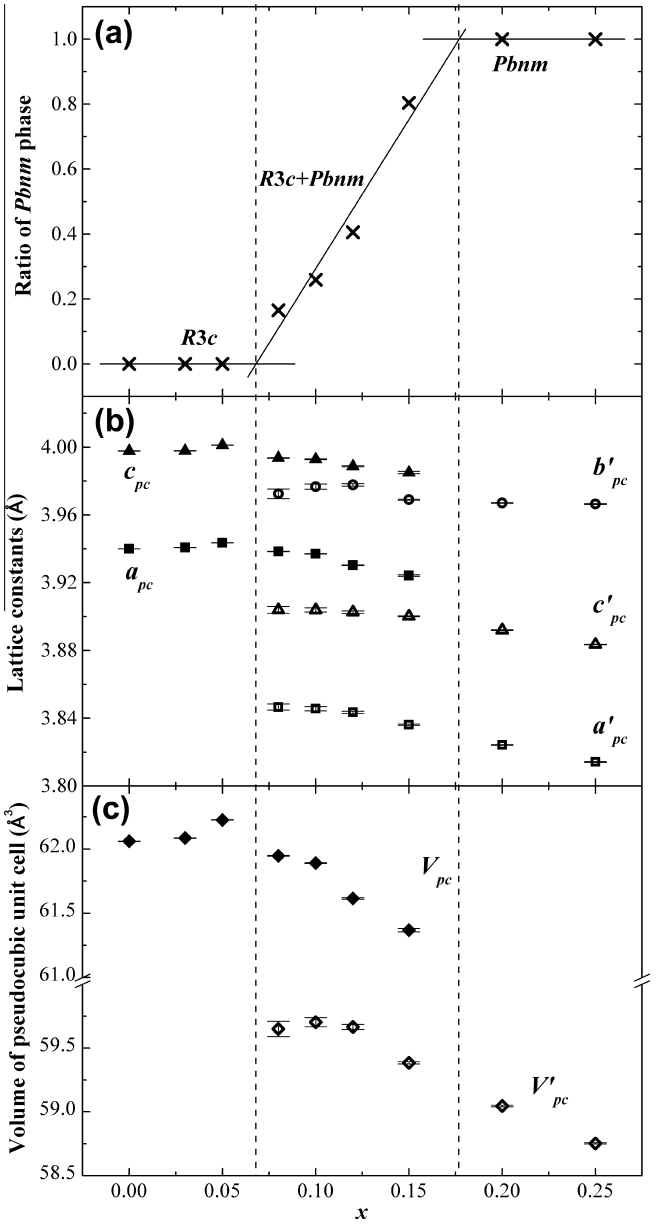

Fig. 2. (a) The ratio of the *Pbnm* phase, (b) the lattice constants and (c) the volume of the pseudocubic unit cell as the function of the doping concentration x. Here the lattice constants and the volumes of the pseudocubic unit cell are calculated with $a_{pc} = a/\sqrt{2}$, $c_{pc} = c/2\sqrt{3}$, $V_{pc} = V/6$ for the *R*3*c* phase and $a'_{pc} = a'/\sqrt{2}$, $b'_{pc} = b'/\sqrt{2}$, $c'_{pc} = c'/2$, $V'_{pc} = V'/4$ for the *Pbnm* phase, where a, c, V, a', b', c' and V' are the lattice constants and the volumes of the primitive cells for the *R*3*c* and *Pbnm* phases, respectively.

of *R*3*c* phase increase slightly, reach their maximums at $x = 0.05$, and then decrease continuously when the *Pbnm* phase emerges. This anomalous lattice expansion in *R*3*c* phase was also observed in low concentration Yb-doped BFO by Yan et al. [15] in spite of the smaller size of Yb^{3+} (1.20 Å) than Bi^{3+} (1.36 Å). On the other hand, the a'_{pc} and c'_{pc} in *Pbnm* phase decrease monotonously with Yb doping, and the b'_{pc} increases slightly and then decreases after $x = 0.12$. Hence the V'_{pc} decreases dramatically after $x = 0.12$.

Raman scattering is a powerful way of investigating ferroelectrics. The high sensitiveness of structural distortion makes it a good supplement of XRD. Unpolarized Raman spectra of BFO and BYFCO powders are presented in Fig. 3. Theoretically, the selection rule gives 13 Raman-active modes of a perovskite-like crystal with *R*3*c* space group: $\Gamma_R = 4A_1 + 9E$. Since each mode can be divided

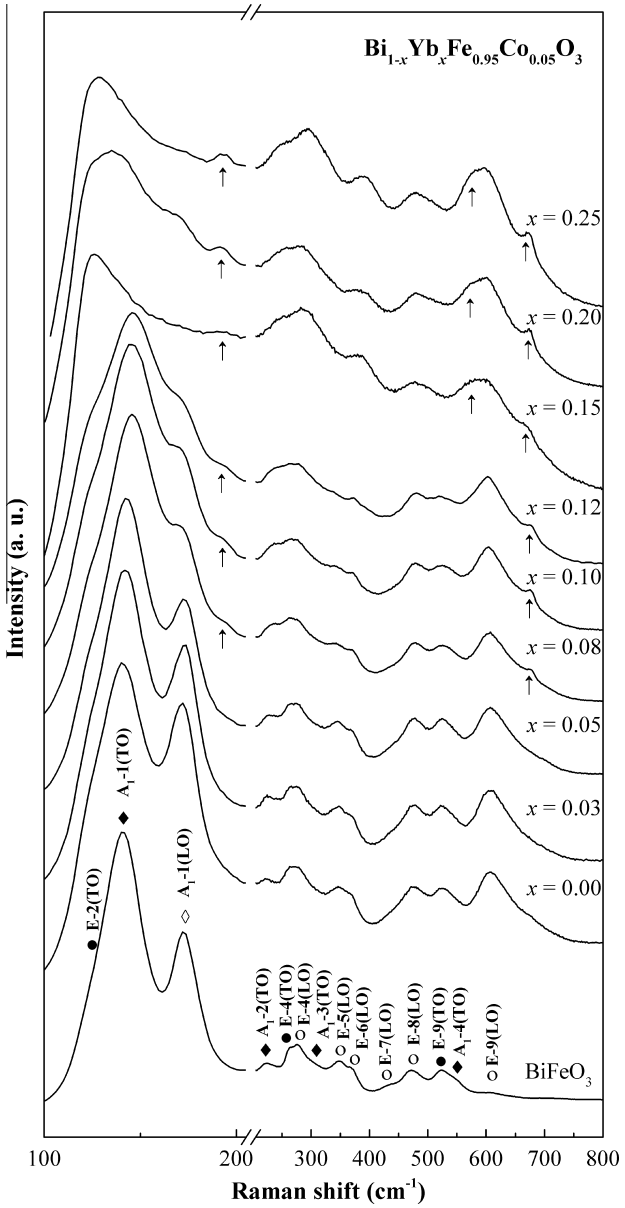

Fig. 3. Raman spectra of BFO and BYFCO powders with different doping concentrations. The assignment of the vibration modes in BFO is consistent with Ref. [16] and the upward arrows indicate the new peaks.

into two vibration types (LO and TO), 26 modes are expected [16]. Analogously, 24 × 2 = 48 modes are expected in the orthorhombic *Pbnm* structure since the selection rule gives: $\Gamma_P = 7A_g + 5B_{1g} + 7B_{2g} + 5B_{3g}$ [17]. Here we observed 14 of the vibration modes in BFO due to the unpolarized limitation, as displaced in Fig. 3. The spectra of BYFCO are similar to that of BFO when $x < 0.08$, accompanied with the reduced A_1-1(LO) mode at 172 cm^{-1} and enhanced E-9(LO) mode at 606 cm^{-1}. The A_1-2(TO) mode at 220 cm^{-1} shifts slightly towards higher wavenumber. When $x \geqslant 0.08$, new vibration modes emerge at 190 cm^{-1} and 680 cm^{-1}, and the A_1-2(TO) mode is broadened due to the transition towards the orthorhombic *Pbnm* phase. With the further increasing Yb^{3+} content to $x = 0.15$, another new vibration mode emerges at 570 cm^{-1} while the A_1-1(TO) mode at 140 cm^{-1} and A_1-1(LO) mode at 172 cm^{-1} are concealed by the rapid enhancement of E-2(TO) mode at 121 cm^{-1}. Meanwhile the E-5(LO) mode at 348 cm^{-1} and E-9(TO) mode at 523 cm^{-1} become undetectable after $x = 0.15$. Obviously three regions can be distinguished based on the Raman spectra, in line with the XRD patterns and the refinement.

It is widely accepted that low frequency Raman modes are dominated by Bi-related vibrations [11,17]. In particular, the A_1-1(LO) mode at 172 cm^{-1} is overlapping with Bi off-center displacement caused by the activation of Bi lone pair [17]. The evolution of the A_1-1(LO) mode indicates that the activation of Bi lone pair is weakened with Yb doping leading to smaller displacement of Bi atom, which might influence the ferroelectric properties of BFO. As a result, BYFCO transforms from the ferroelectric *R*3*c* phase to the centrosymmetric paraelectric *Pbnm* phase. The suppression of the A_1-1(LO) and A_1-1(TO) mode was also reported in a temperature-dependent Raman study around T_c, where a ferroelectric-paraelectric transition occurs [18]. The rapid enhancement of the A-side vibration E-2(TO) mode for $x \geqslant 0.15$ is probably due to the rearrangement of the Bi–O coordination along with the phase transition [17]. On the other hand, it was calculated that the A_1-2(TO) mode at ~220 cm^{-1} is related to the $a^-a^-a^-$ oxygen displacement vector which represents the oxygen octahedral tilt (rotation along [1 1 1] axis) in the *R*3*c* phase [17,19]. It was found that the increase of the oxygen octahedral tilt angle ω is proportional to the blue shift of the A_1-2(TO) mode with a slope of 18 cm^{-1}/deg. [17]. Here, comparing to the BYFCO specimen with $x = 0$, a slight blue shift of the A_1-2(TO) mode with 5.5 cm^{-1} for the BYFCO specimen with $x = 0.05$ is observed. Thus the tilt angle ω is expected to increase by ~0.3°. Furthermore, the tilting of the oxygen octahedra will change the Fe–O–Fe angle. The temperature depended neutron scattering study had shown that a decrease of ω for 0.4° in BFO would induce an increase of Fe–O–Fe angle for 0.6° [8]. In our BYFCO, as Fig. 4 shows, the Fe–O–Fe angle decreases from 153.72° ($x = 0$) to 153.35° ($x = 0.05$), indicating an increase of ω for ~0.24°, in agreement with the result from Raman scattering [20].

It is known that the microscopic crystal distortions have an impact on the DM interaction and thus the spin canting and the cycloid arrangement [9]. Theoretically, direction of the DM vector is determined by the sense of rotation of the oxygen octahedra ω [6]. The increase of ω would increase the canting of the magnetic sublattices, which enhance the DM interaction, and suppress the spin cycloid [9]. This leads to an augment of the macroscopic magnetization.

Integrated hysteresis loops of BFO and BYFCO specimens measured at room temperature are presented in the inset of Fig. 4. The M–H curve of BFO is almost linear with very small remanent magnetization $M_r = 0.014$ emu/g. Clear hysteresis loops can be observed in the BYFCO specimens. The remanent magnetizations M_r of BYFCO are displayed in Fig. 4. The remanent magnetization M_r

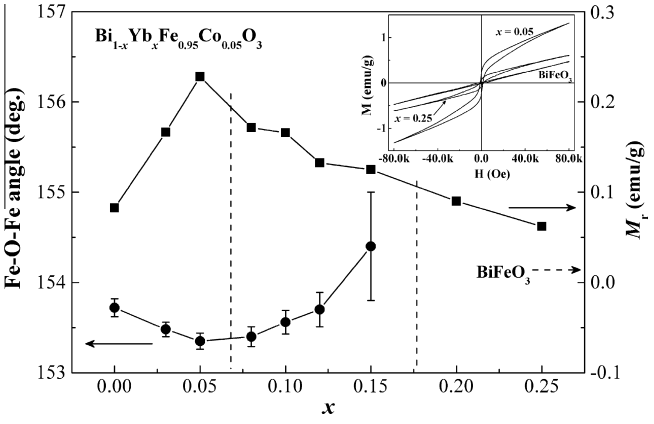

Fig. 4. The remanent magnetization M_r of BYFCO powders and the Fe–O–Fe angle of the *R*3*c* lattices as the function of the doping concentration *x*. The inset shows the hysteresis loops of BFO and BYFCO with $x = 0.05$ and $x = 0.25$.

increases from 0.083 emu/g (for $x = 0$) to the maximum value of 0.228 emu/g (for $x = 0.05$), and starts to decrease as more amount of Yb is doped.

It is known that the magnetic properties of BFO depend significantly on the size of the nanoparticles when the sizes of the BFO particles are less than 100 nm [21]. Based on the full widths of half maximum (FWHMs) of the X-ray patterns and the SEM images for the low x samples, the grain sizes of the samples are larger than 100 nm. Thus one cannot attribute the variation of M_r to the grain size effect. Interestingly the variation of $M_r(x)$ is just opposite to that of the Fe–O–Fe angle shown in Fig. 4. As discussed above, the decrease of Fe–O–Fe angle indicates an increase of the rotation of the oxygen octahedra ω, which enhance the DM interaction and suppress the spin cycloid. Thus the enhancement of the remanent magnetization could be attributed to the increase of ω.

It was found that in the orthorhombic La doped BFO, the spin structure is modified towards a collinear antiferromagnetic structure [22,23], which would result in a reduction of the remanent magnetization. Thus, in the biphasic region, the decrease of M_r could be attributed not only to the increase of the Fe–O–Fe angle but also to the appearance of *Pbnm* phase. Finally, the remanent magnetization decreases to 0.062 emu/g (for the *Pbnm* phase BYFCO with $x = 0.25$), which is larger than the M_r for BFO. Similar results were also reported in other RE-doped orthorhombic BFO [11,24–26].

4. Conclusion

In conclusion, the structural and magnetic properties have been investigated in $Bi_{1-x}Yb_xFe_{0.95}Co_{0.05}O_3$ powders prepared by the sol–gel method. The crystal structure changes from rhombohedral *R*3*c* to orthorhombic *Pbnm* via a biphasic region with an increasing doping concentration x, and an anomalous lattice expansion is observed in the low doping region. An increase of the rotation of the oxygen octahedra ω is indicated for $x \leqslant 0.05$ by the Rietveld refinement and Raman scattering analyses. The substantially enhanced remanent magnetization of BYFCO with $x \leqslant 0.05$ can be attributed to the augment of the DM interaction via the increasing ω.

Acknowledgments

This work was supported by the National Natural Science Foundation of China (NSFC Grant Nos. 11104081 and 11174082) and the Fundamental Research Funds for the Central Universities, SCUT (No. 2012zz0078).

References

[1] M. Fiebig, Revival of the magnetoelectric effect, J. Phys. D Appl. Phys. 38 (2005) R123–R152.
[2] W. Eerenstein, N.D. Mathur, J.F. Scott, Multiferroic and magnetoelectric materials, Nature 442 (2006) 759–765.
[3] G. Catalan, J.F. Scott, Physics and applications of bismuth ferrite, Adv. Mater. 21 (2009) 2463–2485.
[4] D. Lebeugle, D. Colson, A. Forget, M. Viret, A.M. Bataille, A. Gukasov, Electric-field-induced spin flop in $BiFeO_3$ single crystals at room temperature, Phys. Rev. Lett. 100 (2008) 227602.
[5] D. Sando, A. Agbelele, D. Rahmedov, J. Liu, P. Rovillain, C. Toulouse, I.C. Infante, A.P. Pyatakov, S. Fusil, E. Jacquet, C. Carretero, C. Deranlot, S. Lisenkov, D. Wang, J.M. Le Breton, M. Cazayous, A. Sacuto, J. Juraszek, A.K. Zvezdin, L. Bellaiche, B. Dkhil, A. Barthelemy, M. Bibes, Crafting the magnonic and spintronic response of $BiFeO_3$ films by epitaxial strain, Nat. Mater. 12 (2013) 641–646.
[6] C. Ederer, N.A. Spaldin, Weak ferromagnetism and magnetoelectric coupling in bismuth ferrite, Phys. Rev. B 71 (2005) 060401.
[7] I. Sosnowska, T. Peterlin-Neumaier, E. Steichele, Spiral magnetic ordering in bismuth ferrite, J. Phys. C: Solid State Phys. 15 (1982) 4835–4846.
[8] A. Palewicz, R. Przenioslo, I. Sosnowska, A.W. Hewat, Atomic displacements in $BiFeO_3$ as a function of temperature: neutron diffraction study, Acta Crystallogr. B 63 (2007) 537–544.
[9] A.K. Zvezdin, A.P. Pyatakov, On the problem of coexistence of the weak ferromagnetism and the spin flexoelectricity in multiferroic bismuth ferrite, Europhys. Lett. 99 (2012) 57003.
[10] G.L. Yuan, Siu Wing Or, Helen Lai Wa Chan, Structural transformation and ferroelectric-paraelectric phase transition in $Bi_{1-x}La_xFeO_3$ (x = 0–0.25) multiferroic ceramics, J. Phys. D Appl. Phys. 40 (2007) 1196–1200.
[11] Y.J. Wu, J. Zhang, X.K. Chen, X.J. Chen, Phase evolution and magnetic property of $Bi_{1-x}Ho_xFeO_3$ powders, Solid State Commun. 151 (2011) 1936–1940.
[12] A. Gautam, K. Singh, K. Sen, R.K. Kotnala, M. Singh, Crystal structure and magnetic property of Nd doped $BiFeO_3$ nanocrytallites, Mater. Lett. 65 (2011) 591–594.
[13] X.Q. Zhang, Y. Sui, X.J. Wang, Y. Wang, Zh. Wang, Effect of Eu substitution on the crystal structure and multiferroic properties of $BiFeO_3$, J. Alloys Comp. 507 (2010) 157–161.
[14] A.C. Larson, R.B. Von Dreele, General Structure Analysis System (GSAS), Los Alamos National Laboratory Report LAUR 86-748, 2004.
[15] Z. Yan, K.F. Wang, J.F. Qu, Y. Wang, Z.T. Song, S.L. Feng, Processing and properties of Yb-doped $BiFeO_3$ ceramics, Appl. Phys. Lett. 91 (2007) 082906.
[16] J. Hlinka, J. Pokorny, S. Karimi, I.M. Reaney, Angular dispersion of oblique phonon modes in $BiFeO_3$ from micro-Raman scattering, Phys. Rev. B 83 (2011) 020101.
[17] J. Bielecki, P. Svedlindh, D.T. Tibebu, Sh.Zh. Cai, S.G. Eriksson, L. Börjesson, C.S. Knee, Structural and magnetic properties of isovalently substituted multiferroic $BiFeO_3$: Insights from Raman spectroscopy, Phys. Rev. B 86 (2012) 184422.
[18] R. Haumont, J. Kreisel, P. Bouvier, F. Hippert, Phonon anomalies and the ferroelectric phase transition in multiferroic $BiFeO_3$, Phys. Rev. B 73 (2006) 132101.
[19] M. Goffinet, P. Hermet, D.I. Bilc, Ph. Ghosez, Hybrid functional study of prototypical multiferroic bismuth ferrite, Phys. Rev. B 79 (2009) 014403.
[20] Direct extraction of the tilt angle from X-ray diffraction has been done which gives similar tendency that the tilt angle ω reached it's maximum at $x = 0.05$ and decreased with further increasing of x. However, the increasement of the tilt angle $\Delta\omega \sim 1.3°$ is larger than that from Raman data and Fe–O–Fe angles. It is probably that in this direct calculations the distortion from the transverse shift of the oxygen ions might be not excluded.
[21] T.J. Park, G.C. Papaefthymiou, A.J. Viescas, A.R. Moodenbaugh, S.S. Wong, Size-dependent magnetic properties of single-crystalline multiferroic $BiFeO_3$ nanoparticles, Nano Lett. 7 (2007) 766–772.
[22] V.S. Pokatilov, V.V. Pokatilov, A.S. Sigov, Local states of iron ions in multiferroics $Bi_{1-x}La_xFeO_3$, Phys. Solid State 51 (2009) 552–559.
[23] G. Le Bras, D. Colson, A. Forget, N. Genand-Riondet, R. Tourbot, P. Bonville, Magnetization and magnetoelectric effect in $Bi_{1-x}La_xFeO_3$ ($0 \leqslant x \leqslant 0.15$), Phys. Rev. B 80 (2009). 134417.
[24] W.M. Zhu, L.W. Su, Z.G. Ye, W. Ren, Enhanced magnetization and polarization in chemically modified multiferroic $(1-x)BiFeO_3$–$xDyFeO_3$ solid solution, Appl. Phys. Lett. 94 (2009) 142908.
[25] D.V. Karpinsky, I.O. Troyanchuk, M. Tovar, V. Sikolenko, V. Efimov, A.L. Kholkin, Evolution of crystal structure and ferroic properties of La-doped $BiFeO_3$ ceramics near the rhombohedral–orthorhombic phase boundary, J. Alloys Comp. 555 (2013) 101–107.
[26] V.A. Khomchenko, D.A. Kiselev, I.K. Bdikin, V.V. Shvartsman, P. Borisov, W. Kleemann, J.M. Vieira, A.L. Kholkin, Crystal structure and multiferroic properties of Gd-substituted $BiFeO_3$, Appl. Phys. Lett. 93 (2008) 262905.